Microsc. Microanal. 19, S5, 49–53, 2013
doi:10.1017/S1431927613012312

In Situ Heating Transmission Electron Microscopy Observation of Nanoeutectic Lamellar Structure in Sn–Ag–Cu Alloy on Au Under-Bump Metallization

Jong-Hyun Seo,[1,5] Sang-Won Yoon,[2] Kyou-Hyun Kim,[3] Hye-Jung Chang,[1] Kon-Bae Lee,[4] Tae-Yeon Seong,[5] Eric Fleury,[6] and Jae-Pyoung Ahn[1,*]

[1]*Advanced Analysis Center, Korea Institute of Science & Technology (KIST), Hawolgok-dong, Seongbuk-gu, Seoul 136-791, Republic of Korea*
[2]*Electronic Materials Lab, Samsung Corning Precision Materials 644-1, Jinpyeong-dong, Gumi-City, Gyeongsangbuk-do 730-735, Republic of Korea*
[3]*Department of Materials Science and Engineering, University of Illinois at Urbana-Champaign, 1304 W. Green St., Urbana, IL 61801, USA*
[4]*School of Advanced Materials Engineering, Kookmin University, Seoul 136-702, Republic of Korea*
[5]*Department of Materials Science and Engineering, Korea University, Anam-dong 5-1, Seongbuk-gu, Seoul 136-701, Republic of Korea*
[6]*High Temperature Energy Materials Center, Korea Institute of Science & Technology (KIST), Hawolgok-dong, Seongbuk-gu, Seoul 136-791, Republic of Korea*

Abstract: We investigated the microstructural evolution of $Sn_{96.4}Ag_{2.8}Cu_{0.8}$ solder through *in situ* heating transmission electron microscopy observations. As-soldered bump consisted of seven layers, containing the nanoeutectic lamella structure of AuSn and Au_5Sn phases, and the polygonal grains of $AuSn_2$ and $AuSn_4$, on Au-plated Cu bond pads. Here, we found that there are two nanoeutectic lamellar layers with lamella spacing of 40 and 250 nm. By *in situ* heating above 140°C, the nanoeutectic lamella of AuSn and Au_5Sn was decomposed with structural degradation by sphering and coarsening processes of the lamellar interface. At the third layer neighboring to the lamella layer, on the other hand, Au_5Sn particles with a zig-zag shape in AuSn matrix became spherical and were finally dissipated in order to minimize the interface energy between two phases. In the other layers except both lamella layers, polycrystal grains of $AuSn_2$ and $AuSn_4$ grew by normal grain growth during *in situ* heating. The high interface energy of nanoeutectic lamella and polygonal nanograins, which are formed by rapid solidification, acted as a principal driving force on the microstructural change during the *in situ* heating.

Key words: *in situ* heating, Sn–Ag–Cu solder, UBM, microstructure, TEM, STEM

Introduction

Eutectic and near-eutectic solders containing Sn and Pb had been frequently used in the past, because of their low cost, low melting point, and superior mechanical properties (Kim & Tu, 1996; Tu & Zeng, 2001). However, since the use of all hazardous substances in electronic devices was prohibited by Restriction of Certain Hazardous Substances Directive announced in 2006, lead-free Sn-based solder alloys have been commonly developed in packaging materials of electronic devices (Abtew & Selvaduray, 2000; Kim et al., 2003; Ho et al., 2007; Tang et al., 2008; Chinnam et al., 2011).

Under-bump metallization (UBM) soldering technique is recently applied to the integrated circuits of next-generation semiconductors. In our previous study, the Sn–Ag–Cu UBM solder exhibits the microstructural complexity owing to the rapid quenching rate resulting from small feature size under few tens of micrometers, including various crystal phases, nanoeutectic dendrite structure, and those complex multilayers (Bali et al., 2008). Therefore, it is a critical issue to investigate thermal degradation behaviors of the UBM solder, which can crucially affect the mechanical failure and electrical properties at high temperature (Amagai et al., 2002; Kang et al., 2002; Deng et al., 2005; Keller et al., 2011). However, research results on the mechanisms of microstructural change and phase transition induced by thermal aging of solder have not been reported so far, because it is practically very hard to fabricate a transmission electron microscopy (TEM) sample of the micro-sized UBM bump by conventional TEM sampling methods. In this study, we investigated thermally activated kinetic behavior at the interface between the Sn–Ag–Cu solder and Au plate in the UBM solder through *in situ* heating observations of a TEM sample prepared by focused ion beam (FIB) milling technique.

Materials and Methods

Lead-free $Sn_{96.4}Ag_{2.8}Cu_{0.8}$ solder was melted at ~270°C using a diode laser beam with the wavelength of 1,084 nm. The molten solder was then impinged onto the Au (~2-μm-thick)-plated Cu bond pads under N_2 atmosphere at room temperature. The solidification time was ~20 ms, thus resulting in a rapid quenching rate of the order of 10^4 K/s. A TEM sample was fabricated by FIB ion milling, and then was mounted on a TEM heating holder (Gatan 625) for the

© MICROSCOPY SOCIETY OF AMERICA 2013
*Corresponding author. E-mail:jpahn@kist.re.kr

https://doi.org/10.1017/S1431927613012312 Published online by Cambridge University Press

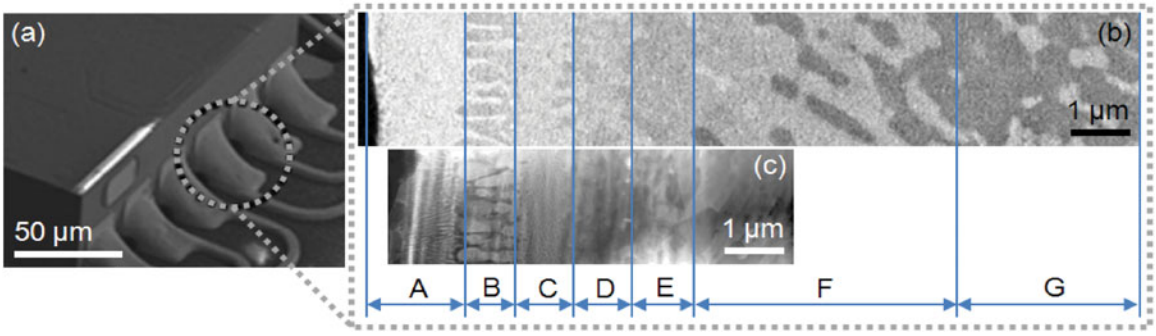

Figure 1. a: A scanning electron microscopy (SEM) image of a packaged under-bump metallization solder, (**b**) a cross-sectional SEM image, and (**c**) a transmission electron microscopy image observed after focused ion beam ion milling, which is corresponding to (**b**) in position and magnification.

in situ heating TEM and scanning TEM (STEM) observations up to 180°C. The phase and composition in each layer of the UBM solder was determined by convergent beam electron diffraction characterizations and energy-dispersive spectroscopy measurements in TEM nanoprobe mode, respectively.

Results and Discussion

Figure 1 shows a scanning electron microscopy (SEM) image of a packaged UBM solder (Fig. 1a), and the cross-sectional SEM (Fig. 1b) and TEM (Fig. 1c) images observed after FIB ion milling. The Figures 1b and 1c have one-to-one correspondence in the microstructure. In the UBM solder solidified at 220°C, which is a solidus temperature of the UBM solder, various eutectic phases, which can be observed in binary Au–Sn alloy, were formed along the rapid heat flux. As shown in Figures 1b and 1c, the solder is distinguished by seven layers (A–G), which was thermodynamically interpreted in our previous work (Bali et al., 2008). The six layers (A–F) can be observed in Figure 1c, but Layer G was unfortunately milled away during TEM sampling by FIB. Through our previous result (Bali et al., 2008) and more detailed TEM observations in this study, we can precisely identify the crystallographic information of each layer. Layers A and B consist of fine and coarse lamellar structures, respectively, with the eutectic phases of Au_5Sn and AuSn. Although Layer C has the same eutectic phases of Au_5Sn and AuSn as Layers A and B, it has a normal casting structure rather than a lamellar structure. In the Layers D and E, polycrystals and equiaxed grains are developed at each layer with different phases of orthorhombic $AuSn_2$ and $AuSn_4$. The $AuSn_4$ phase in Layer E shows a different growth behavior in Layer F, where the $AuSn_4$ phase protrudes into Sn matrix in Layer G. In the final Layer G, the $AuSn_4$ grains are isolated in Sn matrix. The characteristics of microstructural change and phase transition observed during *in situ* heating of as-soldering were summarized in Table 1, including *in situ* TEM results at 140 and 180°C. Unlike the SEM image (Fig. 1b), the Layer A of Figures 1c, 2, and 3 consists of an interesting nanoeutectic structure.

Figure 2 shows the overall microstructure change of UBM solder during the *in situ* heating of an FIB-milled TEM sample, which is the first report on thermal behavior of UBM solder with elevated temperature. Up to *in situ* heating of 120°C, all layers of the UBM solder (Fig. 2a) are

Table 1. The Characteristics of Phase Transition and Microstructural Change of Layers A–G Revealed through *In Situ* Heating Transmission Electron Microscopy (TEM) Observations of the Under-Bump Metallization (UBM) Solder in Figure 1c.

Layer	100°C	140°C	180°C
A	Nanosize eutectic dendrite of Au_5Sn and AuSn	Dissociation of lamellar wall for reducing interface energy	Dissociation of nanosize lamellar
B	Normal eutectic dendrite of Au_5Sn and AuSn	Dissolution of Au_5Sn nanoparticles in AuSn	Complete dissolution of Au_5Sn nanoparticles in AuSn
C	AuSn including isolated Au_5Sn with zig-zag shape	Growth of isolated Au_5Sn by Oswald ripening	$AuSn_2$ polycrystalline growth into AuSn single crystal
D	Equiaxed $AuSn_2$		Elongated $AuSn_2$
E	Equiaxed $AuSn_4$		Equiaxed $AuSn_4$
F	Coarse dendritic structure with ~1-μm-thick dendrites of $AuSn_4$ growing into Sn matrix		Growth of $AuSn_4$ grain
G	Isolated $AuSn_4$ in Sn matrix		

https://doi.org/10.1017/S1431927613012312 Published online by Cambridge University Press

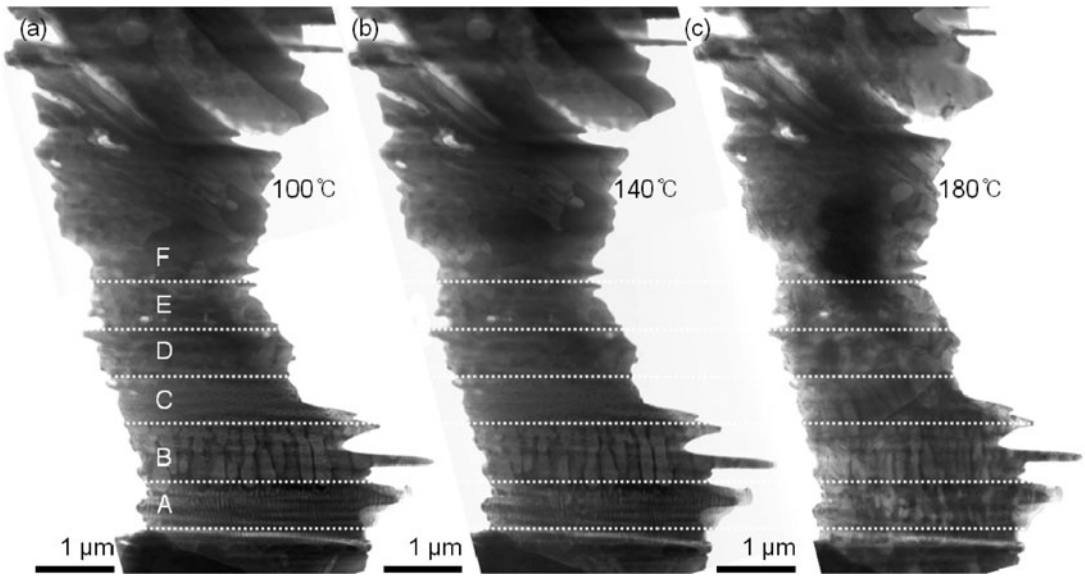

Figure 2. Microstructural change of under-bump metallization solder acquired during *in situ* heating at (**a**) 100°C, (**b**) 140°C, and (**c**) 180°C.

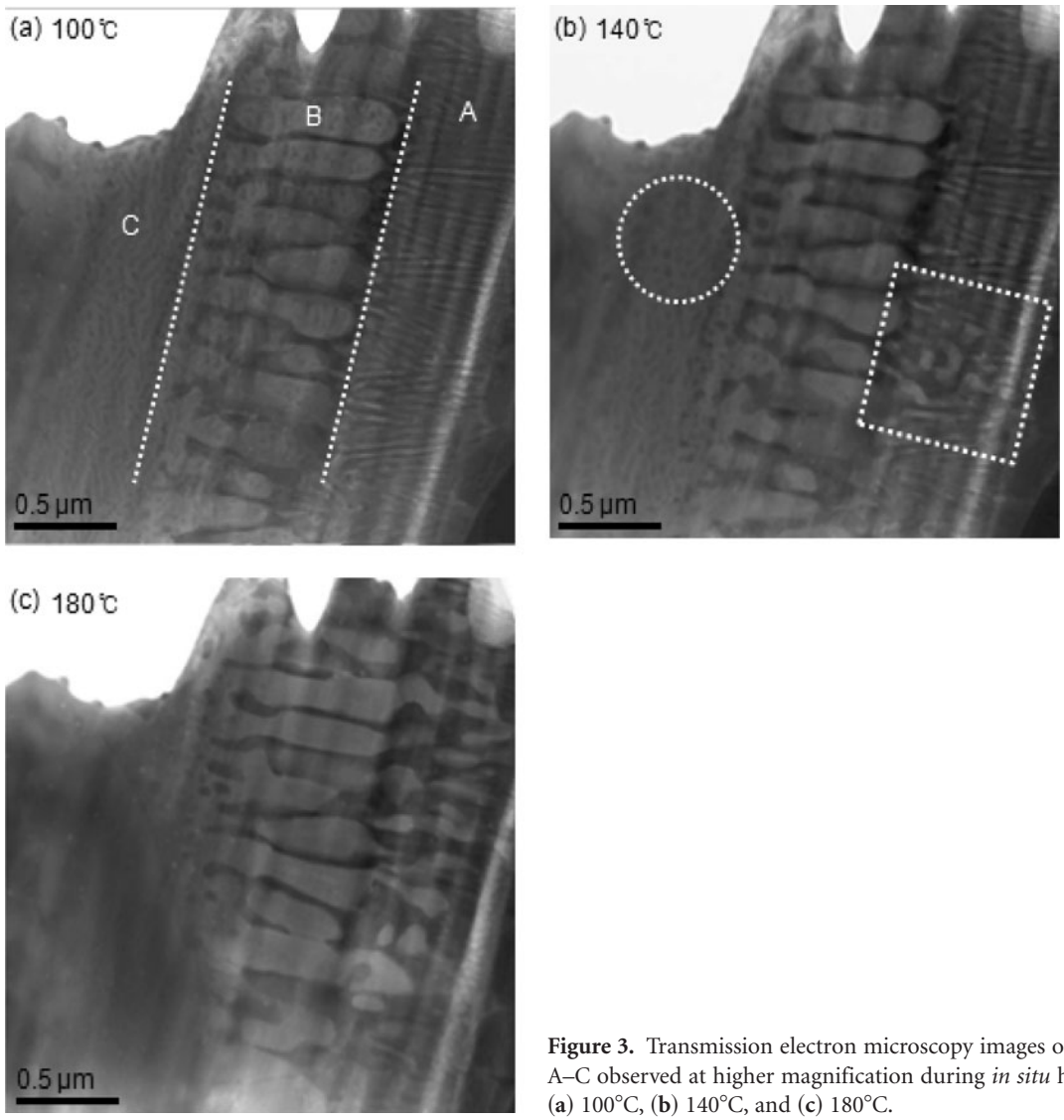

Figure 3. Transmission electron microscopy images of Layers A–C observed at higher magnification during *in situ* heating at (**a**) 100°C, (**b**) 140°C, and (**c**) 180°C.

https://doi.org/10.1017/S1431927613012312 Published online by Cambridge University Press

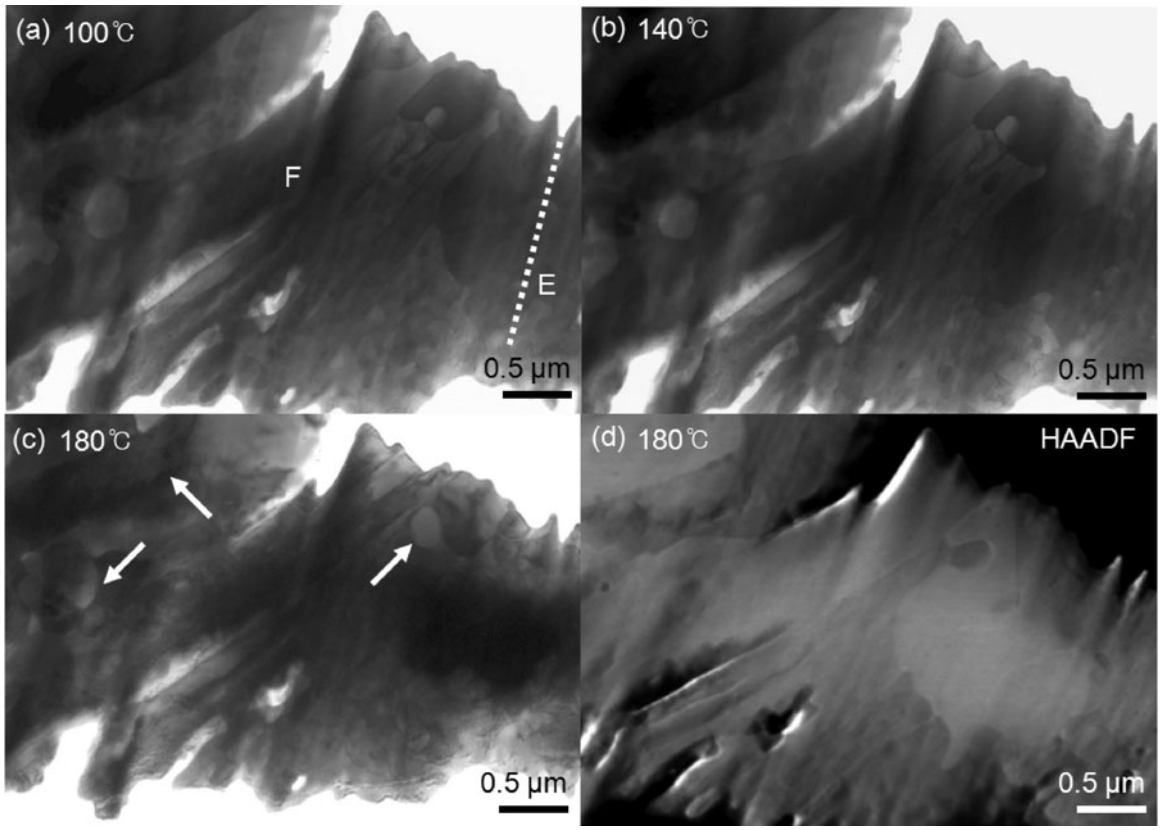

Figure 4. Transmission electron microscopy images of Layers E and F observed at higher magnification during *in situ* heating at (**a**) 100°C, (**b**) 140°C, and (**c**) 180°C, (**d**) high-angle annular dark-field (HAADF) image of (**c**), which the brighter contrast indicates $AuSn_4$ phase and the dark gray contrast is Sn matrix.

scarcely changed from as-solder. A notable small change begins at the nanoeutectic structure of Layer A at 140°C (Fig. 2b), but unfortunately it is not observed in the Figure 2b owing to a low magnification (see Fig. 3b for more detail). On the other hand, microstructural change of other layers is negligible. At 180°C, as shown in Figure 2c, all layers show remarkable change. The nanolamellar structure is collapsed and the interfaces between Layers B, C, and D migrate. The detailed observations on the phase and microstructural evolution of each layer during *in situ* heating will be explained in Figures 3 and 4 through TEM and STEM observation.

Figure 3 shows Layers A–C observed at higher TEM magnification during *in situ* heating. Layers A, B, and C consist of two binary phases of AuSn and Au_5Sn with different structure, showing a gray contrast for AuSn and a dark contrast for Au_5Sn. At 100°C (Fig. 3a), Layers A and B consist of a nanoeutectic lamellar structure of AuSn and Au_5Sn, but Layer A has extremely small interlamellar spacing of 40 nm, compared with thick interlamellar spacing of 250 nm for Layer B. In Layer B, interestingly, the AuSn columnar contains Au_5Sn nanoparticles distributed like small dark spots, which may be formed from an Au-rich area trapped locally in AuSn owing to rapid quenching. Layer C shows a eutectic structure having Au_5Sn islands of zig-zag shape in the AuSn phase. The unique eutectic structure emerges when the contents of Au in AuSn during solidification are low, so that lamellar structure cannot be formed and thereby Au_5Sn nanoparticles should be precipitated. The zig-zag shape indicates that crystallographically specific orientation relationship exists between matrix AuSn and precipitated Au_5Sn (Bali et al., 2008). At 140°C, the nanoeutectic lamellar structure of the Layer A begins to collapse as shown in a rectangle of Fig. 3b. Even though the lamellar structure of Layer B seems to be more stable than that of Layer A at the same temperature, Au_5Sn nanoparticles in lamellar AuSn phase disappear by dissociation of Au_5Sn and diffusion of the dissociated Au atoms into lamellar walls. On the other hand, Au_5Sn nanoparticles in Layer C lose the zig-zag shape by the decomposition and diffusion mechanism same as Au_5Sn in AuSn of Layer B (indicated by the circle in Fig. 3b). The dissipation mechanism of Au_5Sn in Layers B and C is very similar to Oswald ripening phenomena.

At 180°C, the lamellar structure of the Layer A is changed to round shape, of which grains consist of two phases of Au_5Sn and AuSn. Interestingly, it seems to harmonize with Layer B by expanding interlamellar spacing. Layer B shows the lamellar structure with a very clear contrast owing to the complete dissipation of Au_5Sn islands in AuSn. A principal driving force leading to the microstructural change of Layers A–C with increasing temperature was due

https://doi.org/10.1017/S1431927613012312 Published online by Cambridge University Press

to the high interface energy between Au_5Sn and AuSn. Therefore, the nanoeutectic lamellar structure might be decomposed at the lowest temperature, because many interfaces formed at the nanoeutectic lamellar structure provide microstructure instability of UBM solder.

Figure 4 shows the magnified TEM images of Layers E and F in Fig. 2, which is rotated by about 90°. Up to an *in situ* heating temperature of 140°C, Layers D–F maintained the initial structure without the microstructural change that occurred in Layers A–C. At 180°C, equiaxed $AuSn_4$ grains in Layer E slightly grew by normal grain growth mechanism, whereas the elongated $AuSn_4$ grains in Sn in Layer F changed to equiaxed shape without phase change, as shown by arrows in Figures 4c and 4d, showing a high-angle annular dark-field image of Figure 4c. Here, the equiaxed single phases of $AuSn_2$ and $AuSn_4$ in Layers D and E are more stable than the two phases of Layer F, including the elongated $AuSn_4$ grains in Sn matrix. Unfortunately, *in situ* heating TEM experiments above 180°C were not performed in this study, because the TEM sample fabricated by FIB was bent at high temperature. In this work, the structural stability of each layer depended on the interface area between grain boundaries or phase boundaries.

Conclusion

We investigated the phase transition and thermal stability of $Sn_{96.4}Ag_{2.8}Cu_{0.8}$ solder manufactured by laser process through *in situ* heating. The microstructure change of UBM solder up to 120°C was scarcely changed. As-soldered bump consisted of seven layers on an Au-plated Cu bond pad, sequentially containing the nanoeutectic lamella structure of AuSn and Au_5Sn phases, the equiaxed grains of $AuSn_2$ and $AuSn_4$, and the elongated $AuSn_4$ grains in Sn matrix. Above an *in situ* heating temperature of 140°C, the lamellar structure of Layer A with the highest interface energy was first decomposed, and had thick lamellar spacing. The Au_5Sn nanoparticles and zig-zag-shaped Au_5Sn islands in AuSn at Layers B and C were thermally decomposed and disappeared by the complete diffusion of the excess Au toward interfaces. At 180°C, the equiaxed $AuSn_2$ and $AuSn_4$ grains in Layers D and E showed normal grain growth behavior, whereas the elongated $AuSn_4$ grains in Sn matrix in Layer F gradually changed to equiaxed shape. In this way, the specific UBM solder manufactured by rapid quenching process showed the various thermal behaviors by thermal activation process to minimize the interface energy at each layer during *in situ* heating.

Acknowledgements

This research was supported by a grant from Fundamental R&D Program for Core Technology of Materials funded by the Ministry of Knowledge Economy, by Pioneer Research Center Program through the National Research Foundation of Korea funded by the Ministry of Education, Science and Technology, and by Priority Research Centers Program through the National Research Foundation of Korea (NRF) funded by the Ministry of Education, Science and Technology (20090093814).

References

Abtew, M. & Selvaduray, G. (2000). Lead-free solders in microelectronics. *Mater Sci Eng* **27**, 95–141.

Amagai, M., Watanabe, M., Omiya, M., Kishimoto, K. & Shibuya, Y. (2002). Mechanical characterization of Sn-Ag-based lead-free solders. *Microelectron Reliab* **42**, 951–966.

Bali, R., Fleury, E., Han, S.H. & Ahn, J.P. (2008). Interfacial intermetallic phases and nanoeutectic in rapidly quenched Sn-Ag-Cu on Au under bump metallization. *J Alloys Compd* **457**, 113–117.

Chinnam, R.K., Fauteux, C., Neuenschwander, J. & Janczak-Rusch, J. (2011). Evolution of the microstructure of Sn-Ag-Cu solder joints exposed to ultrasonic waves during solidification. *Acta Mater* **59**, 1474–1481.

Deng, X., Sidhu, R.S., Johnson, P. & Chawla, N. (2005). Influence of reflow and thermal aging on the shear strength and fracture behavior of Sn-3.5Ag solder/Cu joints. *Metall Mater Trans A* **36**, 55–64.

Ho, C.E., Yang, S.C. & Kao, C.R. (2007). Interfacial reaction issues for lead-free electronics solders. *J Mater Sci: Mater Elec* **18**, 115–174.

Kang, S.K., Choi, W.K., Yim, M.J. & Shih, D.Y. (2002). Studies of the mechanical and electrical properties of lead-free solder joints. *J Electron Mater* **31**, 1292–1303.

Keller, J., Baither, D., Wilke, U. & Schmitz, G. (2011). Mechanical properties of Pb-free SnAg solder joints. *Acta Mater* **59**, 2731–2741.

Kim, K.H. & Tu, K.N. (1996). Kinetic analysis of the soldering reaction between eutectic SnPb alloy and Cu accompanied by ripening. *Phys Rev B* **53**, 16027–16034.

Kim, K.S., Huh, S.H. & Suganuma, K. (2003). Effects of intermetallic compounds on properties of Sn-Ag-Cu lead-free soldered joints. *J Alloys Compd* **352**, 226–239.

Tang, W., He, A., Liu, Q. & Ivey, D.G. (2008). Fabrication and microstructures of sequentially electroplated Sn-rich Au-Sn alloy solders. *J Electron Mater* **37**, 837–844.

Tu, K.N. & Zeng, K. (2001). Tin-lead (SnPb) solder reaction in flip chip technology. *Mater Sci Eng R-Rep* **34**, 1–58.

https://doi.org/10.1017/S1431927613012312 Published online by Cambridge University Press